SOLID RUBBER FENDERS TO PREVENT STRUCTURAL DAMAGE IN A LOW-SPEED COLLISION BETWEEN A SHIP-SHAPED OFFSHORE INSTALLATION AND A SHUTTLE TANKER WORKING SIDE-BY-SIDE IN OFFLOADING OPERATION

Reference NO. IJME 1218, DOI No: 10.5750/ijme.v165iA2.1218

H J Kim, University College London, UK; Pusan National University, South Korea, **S M Park**, The International Centre for Advanced Safety Studies (Lloyd's Register Foundation Research Centre of Excellence) at KOSORI, South Korea, **G Thomas**, University College London, UK and **J K Paik***, University College London, UK; Ningbo University, China; Yantai Research Institute of Harbin Engineering University, China; The International Centre for Advanced Safety Studies (Lloyd's Register Foundation Research Centre of Excellence) at KOSORI, South Korea.

* Corresponding author. J K Paik (Email) j.paik@ucl.ac.uk

KEY DATES: Submission date: 13.10.2022 / Final acceptance date: 13.07.2023 / Published date: 27.11.2023

SUMMARY

Ships and ship-shaped offshore installations are commonly equipped with pneumatic or solid rubber fenders to absorb kinetic energy during collisions, thereby reducing structural damage. The energy absorption capacity of these fenders must be precisely evaluated via reliable experimental, analytical, and numerical methods to ensure that the fenders are capable of preventing collision-associated structural failures. Accordingly, this study developed computational modelling techniques for analysing the energy absorption capacity of solid rubber fenders. Modelling was performed using LS-DYNA, a commercial software package for finite element simulation, and the developed models were validated by comparison with data from crushing tests on two types of solid rubber fender models – circular tube and V-shaped rubber fenders. The validated computational models were applied to examine a case study of a low-speed collision between a Suezmax class shuttle tanker and a very-large-crude-oil-carrier (VLCC) class ship-shaped offshore installation working side-by-side in offloading operation, with the latter equipped or not equipped with V-shaped rubber fenders, respectively. The results revealed that such fenders were effective protection against structural damage in such a collision scenario.

KEYWORDS

Ship-shaped offshore installation; Shuttle tanker; Side-by-side offloading; Low-speed collisions; Solid rubber fender

1. INTRODUCTION

Marine accidents can result in injury, loss of life or property, or damage to the marine environment. Thus, advanced technologies must be developed to minimise the risk of such accidents and thereby protect people, property and the environment (Paik, 2018, 2020, 2022). Collisions are a typical marine accident that continues to occur despite preventive efforts and can cause catastrophic structural damage and marine pollution (Faisal et al., 2017; Kim et al., 2021; Ko et al., 2018a; Paik et al., 2017b; Youssef et al., 2016).

Many studies have examined collisions between ships and offshore platforms (Babaleye and Kurt, 2020; Cho et al., 2023; Deeb et al., 2017; Dekker and Walters, 2017; Fernandez et al., 2022; Haris and Amdahl, 2012; Jones and Paik, 2013; Kim et al., 2021; Ladeira et al., 2022; Liu et al., 2018; Paik, 2007a, 2007b; Paik and Thayamballi, 2006; Park et al., 2023; Quinton et al., 2017; Samuelides, 2015; Shokrgozar et al., 2022; Storheim and Amdahl, 2017; Yu et al., 2019; Zhang et al., 2015), and between ships and bridges (Chen et al., 2022; Pan et al., 2022; Sha and Amdahl, 2019; Song and Wang, 2019; Wu et al., 2019; Zhang et al., 2014). Among them, the group of the authors (Paik, 2022; Park et al., 2023) studied the ability of "pneumatic" rubber fenders to protect a ship-shaped offshore installation and a shuttle tanker working side-by-side in offloading conditions (Figure 1) from suffering damage as a result of collisions. They noted that this damage includes minor structural damage to hull structures, such as local denting. Low-speed collisions are one of the most frequent types of accidents at sea, accounting for approximately 20% of global marine accidents (Cefor, 2021). Moreover, continual low-speed collisions lead to the accumulation of structural damage, which can considerably reduce structural integrity and necessitate expensive on-site repairs.

Rubber fenders are widely used in the marine industry because they exhibit large deformations under small loads, which enables them to absorb kinetic energy during collisions (Woo and Park, 2019; Woo et al., 2002).

Figure 1. A ship-shaped offshore installation and a shuttle tanker working side-by-side in offloading operations (Paik, 2022; Park et al., 2023)

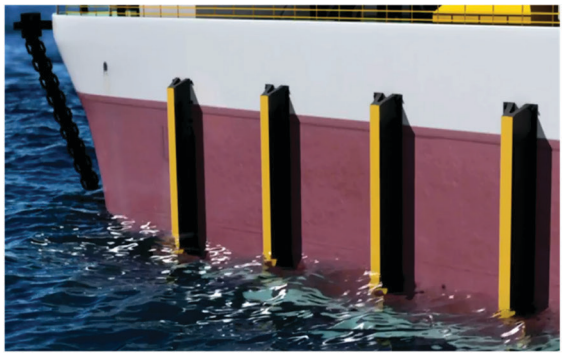

Proposed schematic (Trelleborg, 2023)

Applied example: PETROBRAS 68 FPSO (OilNOW, 2023)

Applied example: JANGKRIK FPU

Figure 2. Solid rubber fenders installed onto the side structures of ship-shaped offshore installations

"Pneumatic" rubber fenders have typically been used to prevent structural damage caused by collisions during side-by-side offloading operations involving a ship-shaped offshore installation and a shuttle tanker. However, in recent years, solid rubber fenders with a shape of hollow-section or others have been installed onto the hulls of large ship-shaped offshore installations, such as floating production, storage, and offloading (FPSO) units and floating liquefied natural gas (FLNG) units, to prevent such collision-associated damages, as shown in Figure 2.

Compared with "pneumatic" rubber fenders, solid rubber fenders have advantages (Trelleborg, 2023) as they are:

- easier to maintain and replace,
- more durable,
- have lower friction, and
- are less expensive.

Studies have investigated the mechanical behaviour and energy absorption capacity of solid rubber fenders under various loads. Regarding rubber fenders subjected to lateral loads, Lee and Park (2012) numerically analysed rubber fenders to identify their energy absorption characteristics. They also introduced a thickness ratio of T_r / T_m for rubber fender design – where T_r is rubber fender thickness and T_m is monopile thickness – and suggested that T_r / T_m should be greater than 8 for meteorological mast structures. Lee (2013) investigated the suitable size and composition for the rubber fender of a tripod offshore wind turbine under various collision scenarios. Ali et al. (2017) analytically evaluated the response of solid rubber fenders under dynamic loads. Rudan et al. (2021) used the Mooney–Rivlin hyperelastic constitutive model to analyse the function of solid rubber fenders installed on a moored floating storage regasification unit. Cho et al. (2023) studied the effect of solid rubber fenders on structural damage due to collisions between an FPSO unit hull and an offshore supply vessel. Regarding rubber fenders subjected to axial compressive loads, Akiyama et al. (2017a, 2017b) have conducted a series of compression tests to evaluate the service life of large aging solid rubber fenders. Wu and Chiou (2019) experimentally analysed the mechanical behaviour of a circular tube-shaped rubber fender under monotonic and cyclic compressive loads. Similarly, Shen et al. (2020) experimentally and numerically investigated the stress–strain response and buckling behaviour of circular tube-shaped rubber fenders with various wall thicknesses under monotonic and cyclic compressive loads. Shen et al. (2022) experimentally investigated the effect of V-notch ring grooves on the energy absorption capacity of circular tube-shaped rubber fenders.

Although the above-mentioned studies have presented valuable findings, it is obvious that there are still a lot of technical issues to be resolved for safety design and engineering in collisions in association with accurate and efficient computations of the mechanical behaviour and energy absorption capacity of solid rubber fenders.

Under increasing axial compressive loads, the crushing behaviour exhibited by solid rubber fenders is similar to that exhibited by thin-walled steel structures (Paik, 2018, 2020, 2022). Figure 3 presents the experimental and numerical results obtained from the present study, which experimentally investigated the crushing characteristics and thus the energy absorption capacities of solid rubber fenders. Crushing tests were conducted on both circular tube and V-shaped rubber fenders. The circular tube-shaped fender model tests investigated the local buckling and folding or crushing behaviour of rubber fenders in general, while the V-shaped fender tests investigated more complex crushing behaviour owing to its complex geometry.

Computational modelling techniques were developed and validated using the data obtained from the above-mentioned physical tests. These validated modelling techniques were then used to perform case studies of low-speed collisions between a very-large-crude-oil-carrier (VLCC) class FPSO unit hull and a Suezmax class shuttle tanker.

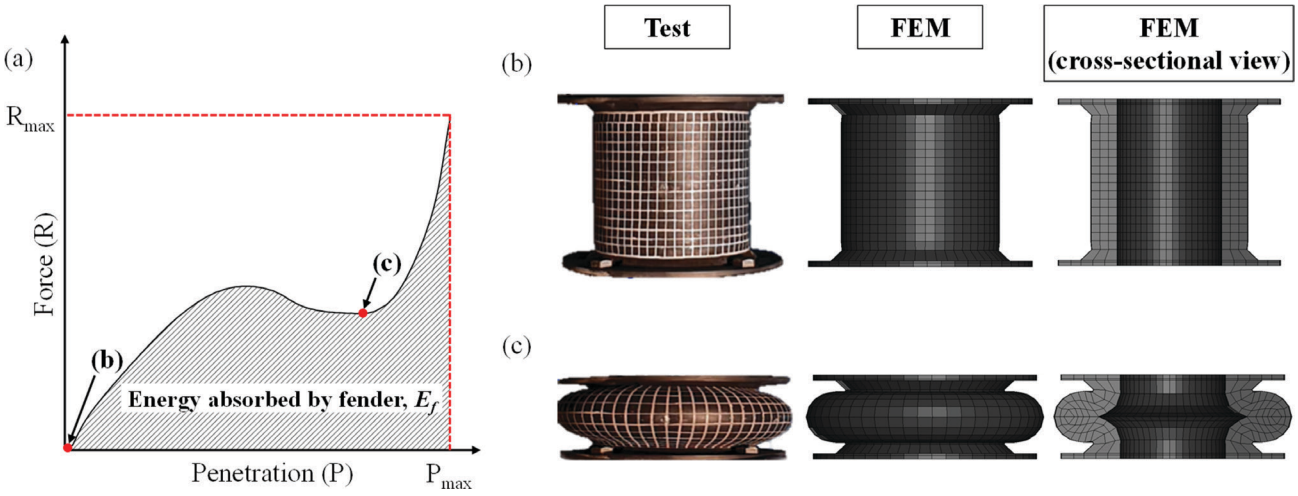

Figure 3. Crushing of a circular tube-shaped rubber fender under predominantly compressive loads: (a) crushing behaviour, (b) initial state, and (c) folded state (FEM = finite element method)

2. COMPUTATIONAL MODELLING TECHNIQUES FOR ANALYSIS OF RUBBER MATERIALS ASSISTED WITH TEST DATA

Rubber material exhibits different characteristics from other engineering materials used in ships and ship-shaped offshore installations. For example, rubber is a hyperelastic material, so its primary mechanical characteristic is elasticity. In addition, rubber exhibits viscoelasticity and incompressibility, and a nonlinear stress–strain relationship in its elastic region. Table 1 compares the mechanical properties of rubber and ordinary steel (Lindley, 1974; Paik, 2022).

Table 1. Mechanical properties of rubber and ordinary steel (Lindley, 1974; Paik, 2022)

Mechanical property (unit)	Rubber	Ordinary steel (grade A)
Density (kg/m^3)	1,200	7,850
Young's modulus (MPa)	5.9	205,800
Shear modulus (MPa)	1.4	81,000
Bulk modulus (MPa)	1,200	176,000
Yield stress (MPa)	-	235
Fracture strain	4.2	0.4
Poisson's ratio	0.499	0.3

The mechanical properties of rubber can vary greatly depending on the composition of precursor rubber compounds and manufacturing quality. Consequently, the mechanical properties of rubber are insufficiently standardised and must be determined for each rubber used in a given construction. In the present study, two different types of data were used to model rubber: data from uniaxial tension tests, and a combination of data from various material tests. This modelling was performed with LS-DYNA, a commercial software package for finite element simulation (www.ansys.com).

2.1 MATERIAL MODELLING UNDER UNIAXIAL TENSILE LOAD

Uniaxial tension tests (also called tensile coupon tests) are the most common material test used to determine the mechanical properties of engineering materials, particularly for determining sufficiently accurate values for use in finite element models of ships and offshore structures. In this study, uniaxial test data and the material model 'MAT 181 (SIMPLIFIED_RUBBER/FOAM)' (hereinafter 'MAT 181') were employed for the computational modelling of rubber. MAT 181 does not require curve fitting; instead, it uses only uniaxial stress–strain curves obtained directly from uniaxial tension testing (Engelbrektsson, 2011). Furthermore, MAT 181 performs linear interpolation of stress–strain curves at varying strain rates, such that it can model structures that exhibit strain rate–dependent responses owing to changes in loading and deformation velocities.

In the present study, however, such strain rate-dependency was not considered in the computational modelling because the effect of strain rates in low-speed collision cases under consideration may be neglected. Further studies are required and a sequel to this paper is ongoing to deal with the effect of strain rates.

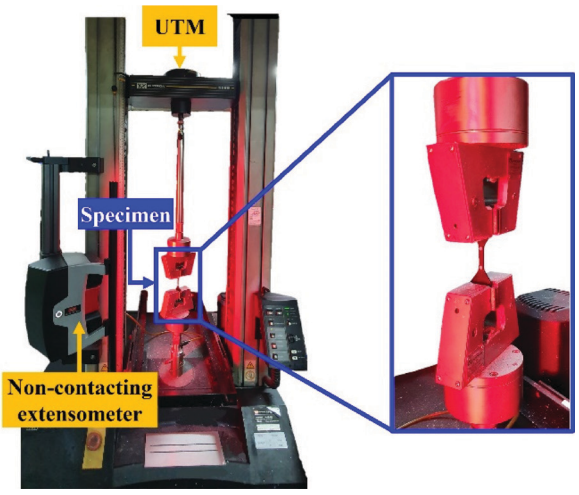

Figure 4. Set-up for uniaxial tension test; the inset shows an expanded view of the mounted rubber specimen (UTM = universal test machine)

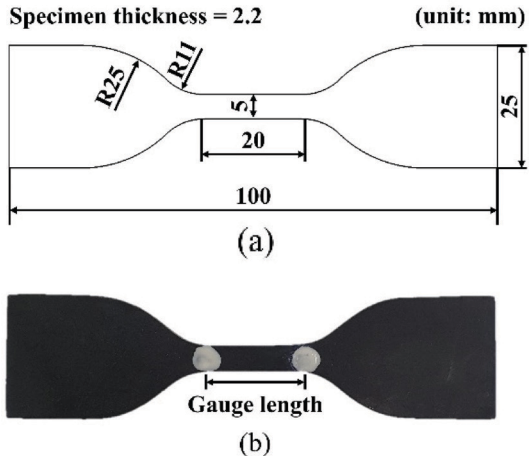

Figure 5. Details of rubber specimen subjected to uniaxial tension test-Type 1A (ISO 37): (a) dimensions, and (b) gauge length

In this study, uniaxial tension tests on rubber were carried out. Figure 4 shows the set-up and a mounted rubber specimen used for the uniaxial tension testing that was performed in the present study. The specimens were extracted from the test specimens used in the physical model testing in section 3, in accordance with the International Organization for Standardization (ISO) 37 specification (ISO, 2017) (Figure 5). Three specimens of each physical testing specimen were tested using a

universal testing machine (UTM) (Instron 5565, Instron, MA, USA), and the strain data were measured using a non-contacting video extensometer that has accuracy of ± 1 μm (Instron, 2005, 2020).

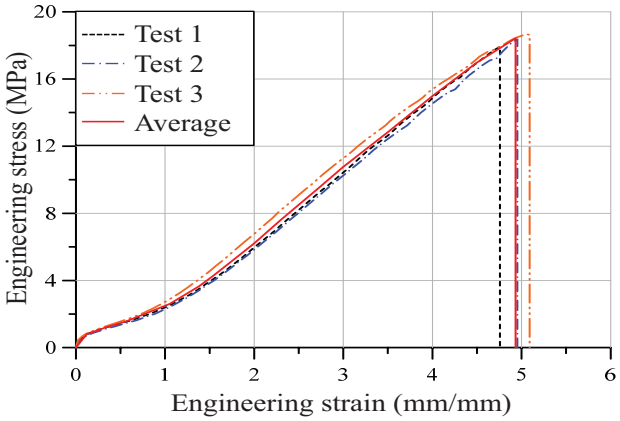

(a) For the circular tube-shaped rubber fender material

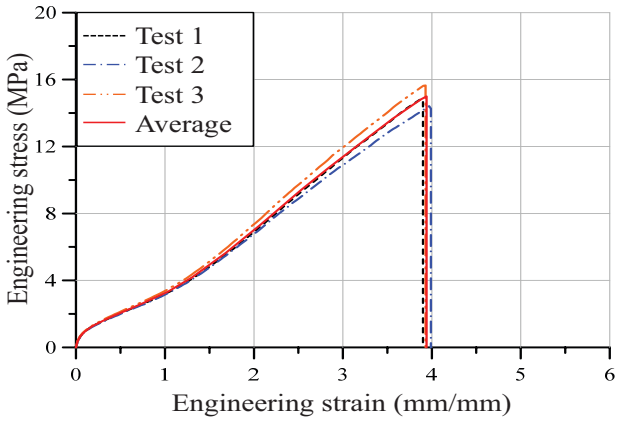

(b) For the V-shaped rubber fender material

Figure 6. Engineering stress–engineering strain curves of rubber specimens at room temperature (20 °C ± 5 °C) obtained from the present study

Figure 6 shows the engineering stress–engineering strain curves obtained from the uniaxial tension testing on rubber materials with two types of rubber fenders – circular tube and V-shaped fenders. The tensile testing was continued until rupture in the first tension loading without repeated deformation and recovery processes, thereby ignoring the Mullins effect, as discussed in Section 3.1(c). Figure 7 shows the specimens after testing.

2.2 MATERIAL MODELLING UNDER COMBINED LOADS

In contrast to steels, rubber exhibits a fully nonlinear stress–strain relationship, which is difficult to characterise using the few properties determined from uniaxial tension tests. In addition, Kim et al. (2004) reported that material properties determined from uniaxial tension testing are ~20% higher than those determined from a combination of data from various material tests, such as uniaxial tension and compression tests, equi-biaxial tension tests, and pure shear tests as depicted in Figure 8 (Woo, 2019).

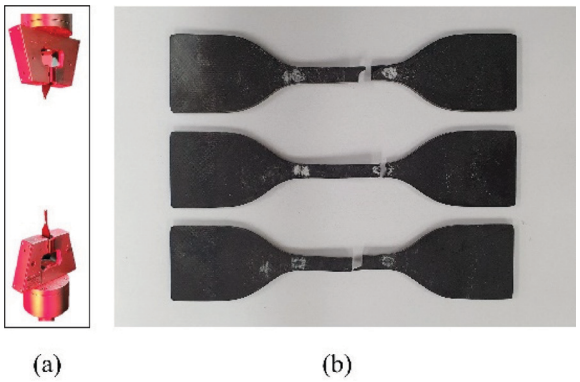

Figure 7. Specimens after uniaxial tension testing conducted in the present study: (a) position at end of testing, and (b) failure shapes

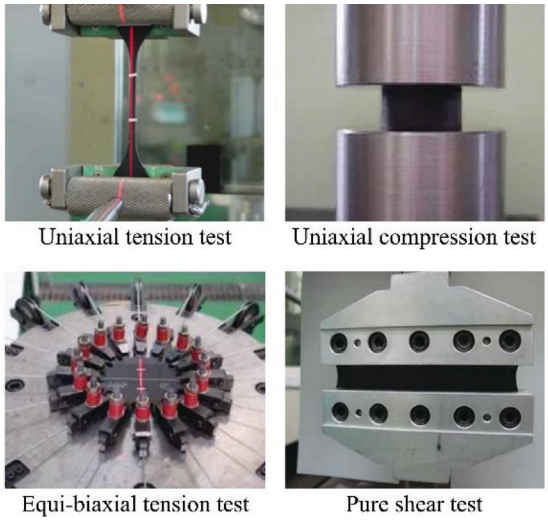

Figure 8. Various material tests conducted on rubber materials (Woo, 2019)

A combination of data from material tests should therefore be made with data from uniaxial tension tests in the finite element analysis (FEA) of solid rubber fenders. Curve-fitting methods are used to combine such data to afford material parameters employed in theoretical constitutive models of hyperelastic materials, such as the Arruda–Boyce, Gent, Mooney–Rivlin, neo-Hookean, Ogden, and Yeoh models, because curve-fitting methods and resulting constitutive models have been recognised as useful (Ali et al., 2010; Beda, 2007, 2014; Dal et al., 2021; He et al., 2022; Melly et al., 2021).

The Ogden and Mooney–Rivlin models of materials are the most commonly used models due to their high accuracy (Ali et al., 2010; Böl and Reese, 2006). However, the Mooney–Rivlin model cannot be used for the analysis

of large deformations (Saidou et al., 2021). Thus, the Ogden model was employed in the current study for the computational modelling of rubber materials using a combination of data from various tests and the 'MAT 77 O-OGDEN_RUBBER' LS-DYNA model, as the Ogden model predicts mechanical behaviour for a wide range of deformations.

The Ogden model of materials uses the strain energy function of principal stretches $_1$, λ_2, and λ_3, as defined below in Equation (1). The manufacturer of the rubber fenders conducted various material tests of specimens and provided us with the material parameters listed in Table 2.

These were determined using the curve-fitting method to combine the test data of stress-strain relationships obtained from uniaxial tension tests, equi-biaxial tension tests, and pure shear tests conducted under quasi-static loading conditions. The various material test data obtained under the first loading were used not to consider the Mullins effect, see Section 3.1 (c). It is noted that repeated deformation and recovery processes are required in the material tests to take into account the Mullins effect.

$$W = \sum_{n=1}^{N} \frac{\mu_n}{\alpha_n}\left(\lambda_1^{\alpha_n} + \lambda_2^{\alpha_n} + \lambda_3^{\alpha_n} - 3\right) \quad (1)$$

where W is the strain energy function, and α_n and μ_n are material parameters that are obtained by curve-fitting.

Table 2. Material parameters of rubber fender specimens

Parameters	Circular tube-shaped fender material	V-shaped fender material
α_1	4.391	3.404
μ_1	0.028	0.167
α_2	0.032	2.024
μ_2	5.814	0.673
α_3	2.589	2.024
μ_3	0.954	0.858

It is obvious that loading speed can significantly affect the properties of materials such as steels or rubbers. However, the present study neglects the effect of strain rates on the mechanical properties of rubber materials because it deals with a low-speed collision case and the resulting strain-rate dependency is supposed to be small. Further studies are required and a sequel to this paper is ongoing to deal with the effect of strain rates on the mechanical properties of rubber materials in high-speed collision cases.

3. TESTING OF PHYSICAL SPECIMENS AND VALIDATION OF COMPUTATIONAL MODELLING TECHNIQUES

Crushing testing with two types of solid rubber fenders – circular tube and V-shaped fenders was conducted in the present study. The specimens were fabricated by Hwaseung Corporation in Busan, Republic of Korea, and consisted of styrene butadiene rubber reinforced with carbon black. They were designed by the manufacturer, in accordance with the guideline provided by the Permanent International Association of Navigation Congresses (PIANC, 2002), to have a maximum energy-absorption efficiency (f) of 52.5% under deformation, where f is defined by Equation (2), as follows:

$$\mathrm{f} = \frac{E_f}{\mathrm{R_{max}P_{max}}} \times 100\ (\%) \quad (2)$$

where E_f is the energy absorbed by the specimen, and $\mathrm{R_{max}}$ and $\mathrm{P_{max}}$ are the maximum force and penetration of the specimen, respectively, as indicated in Figure 3.

3.1 CRUSHING TEST ON CIRCULAR TUBE-SHAPED RUBBER FENDER

3.1 (a) Test Specimen

Figures 9 and 10 show a crushing test specimen on a circular tube-shaped rubber fender with its dimensions, as provided by the manufacturer. Ordinary steel plates were embedded into the end flanges of the test specimen to maintain a flat surface, as shown in Figure 10. The specimen was also perforated with four symmetrically distributed holes, which allowed it to be bolted to the loading actuator.

3.1 (b) Test Set-up

Figures 11 and 12 show schematics of the test equipment arrangement and test set-up at the International Centre for Advanced Safety Studies (ICASS)/Korea Ship and Offshore Research Institute (KOSORI) test site (www.icass.center) in Hadong, Republic of Korea. The 500-kN hydraulic actuator (Figure 13) was fixed to a reaction wall to provide axial compressive loads. First, the jig was coupled between the loading actuator and the specimen to uniformly distribute the compressive loads around the test specimen. Then, the loading actuator was shifted forward, and the opposite end of the specimen was attached to the other side of the reaction wall.

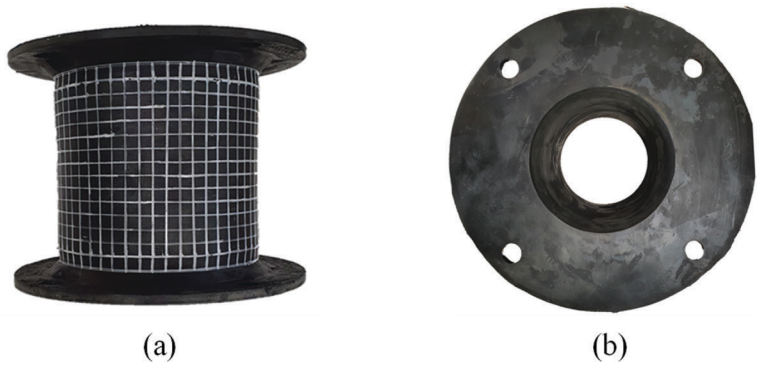

Figure 9. Circular tube-shaped rubber fender used for crushing test: (a) front view, and (b) top view

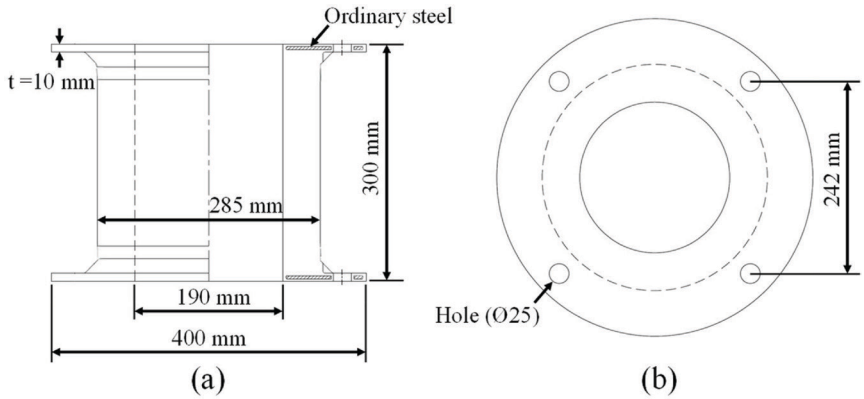

Figure 10. Dimensions of the circular tube-shaped rubber fender crushing test specimen: (a) front view, and (b) top view

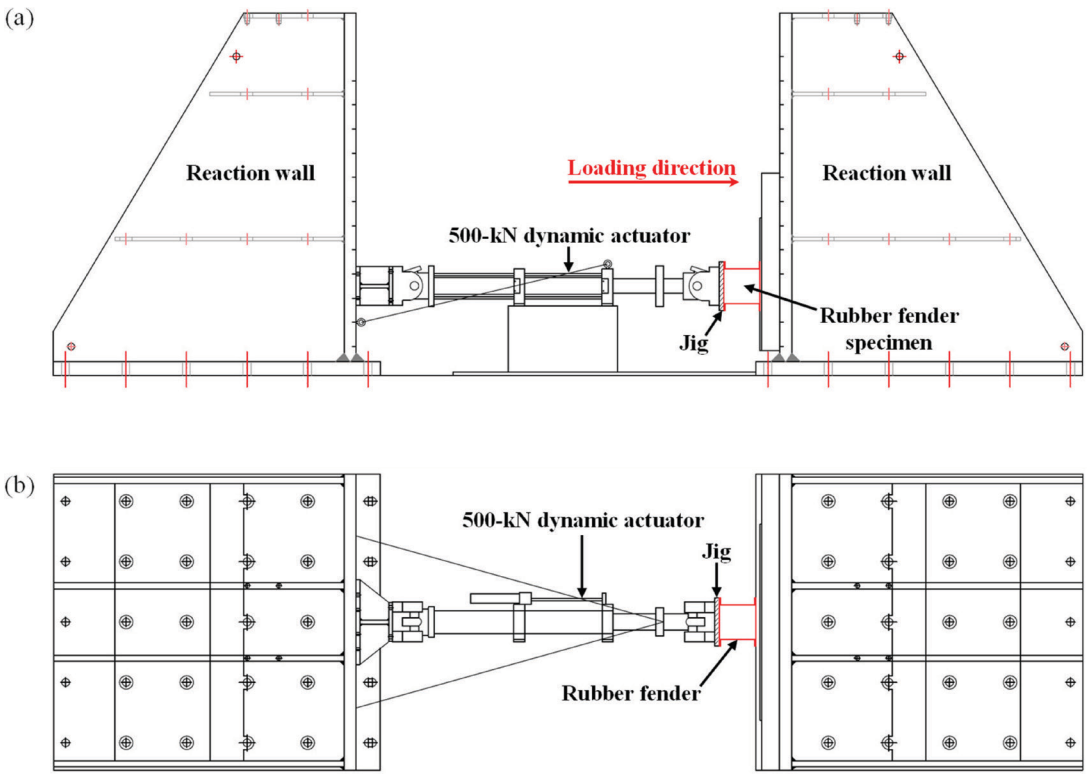

Figure 11. Circular tube-shaped rubber fender crushing test set-up: (a) elevation view, and (b) plan view

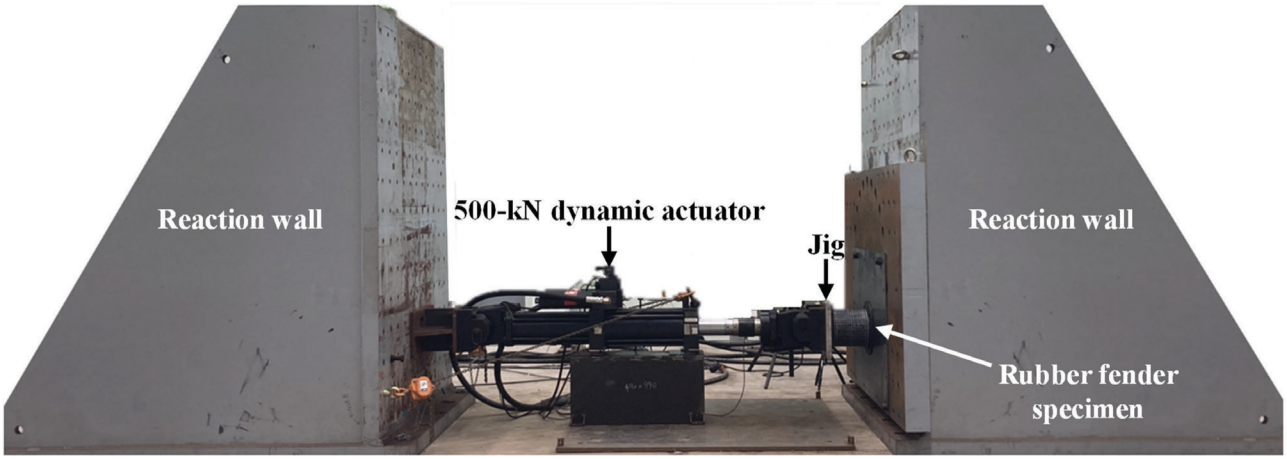

Figure 12. Crushing test set-up of the circular tube-shaped rubber fender before axial compressive loading

A personal computer was used to control the loading speed and displacement of the actuator. The load and stroke signals were measured using a 500-kN load cell and a linear variable displacement transducer (LVDT), respectively.

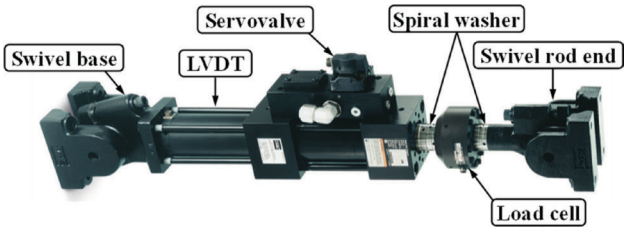

Figure 13. A 500-kN dynamic actuator

3.1 (c) Test Scenario

The circular tube-shaped crushing test was performed under quasi-static compressive loading. A very low loading speed of 0.05 mm/s was used, which corresponds to quasi-static conditions, as described in Chapter 18 of Paik (2020). The test was conducted at room temperature (20 °C ± 5 °C), as rubber is temperature sensitive. As mentioned, the Mullins effect was not considered, as it is challenging to characterise this stress-softening phenomenon under cyclic loading for a given rubber product (Mullins, 1969; Zhang et al., 2021). Furthermore, the softening of rubbers owing to cyclic loading is a temporary phenomenon, as they can recover their stiffness within a few days (Laraba-Abbes et al., 2003; Yan et al., 2010). Thus, as the ship-shaped offshore installations are usually offloaded once a week, the effect of rubber softening on fender performance can be neglected. Consequently, the physical testing was carried out without the stabilisation of structural responses.

3.2 CRUSHING TEST ON V-SHAPED RUBBER FENDER

3.2 (a) Test Specimen

The crushing test on a V-shaped rubber fender model had the same geometry and material properties as the V-shaped rubber fenders installed onto the side shell structures of the PETROBRAS 79 FPSO unit. Figures 14 and 15 show the test specimen and its dimensions, as provided by the manufacturer. Ordinary steel plates were embedded into the top and bottom of the specimen to maintain a flat surface and to enable it to be fixed onto hull structures, as shown in Figure 15.

3.2 (b) Test Set-up

Figure 16 shows the crushing test set-up on the V-shaped rubber fender at the Hwaseung Corporation test site in Yangsan, Republic of Korea.

The specimen was subjected to axial compressive loads in a 10,000-kN hydraulic compression testing press. A jig was used to set the fixed boundary condition on the bottom of the specimen, and a personal computer was used to control the loading speed and displacement of the testing press.

3.2 (c) Test Scenario

The crushing test on the V-shaped rubber fender was performed using the lowest loading speed of the testing press – 0.33 mm/s (20 mm/min) – to represent acceptable quasi-static conditions. As presented in Section 3.1(c), the test was conducted at room temperature (20 °C ± 5 °C) and the Mullins effect was not considered.

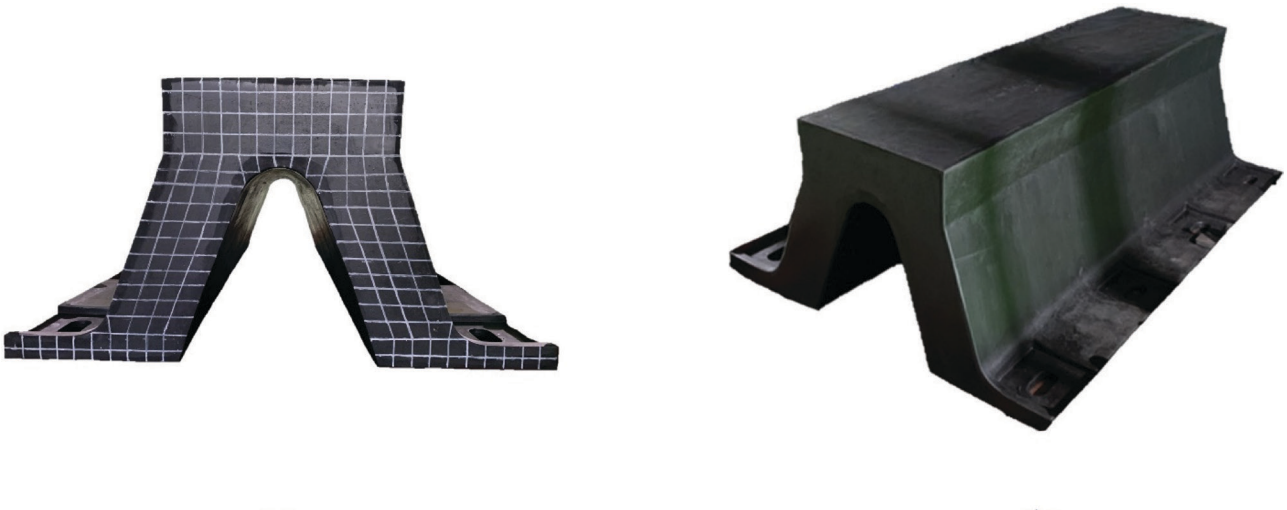

(a) (b)

Figure 14. V-shaped rubber fender used for crushing testing: (a) front view, and (b) isometric view

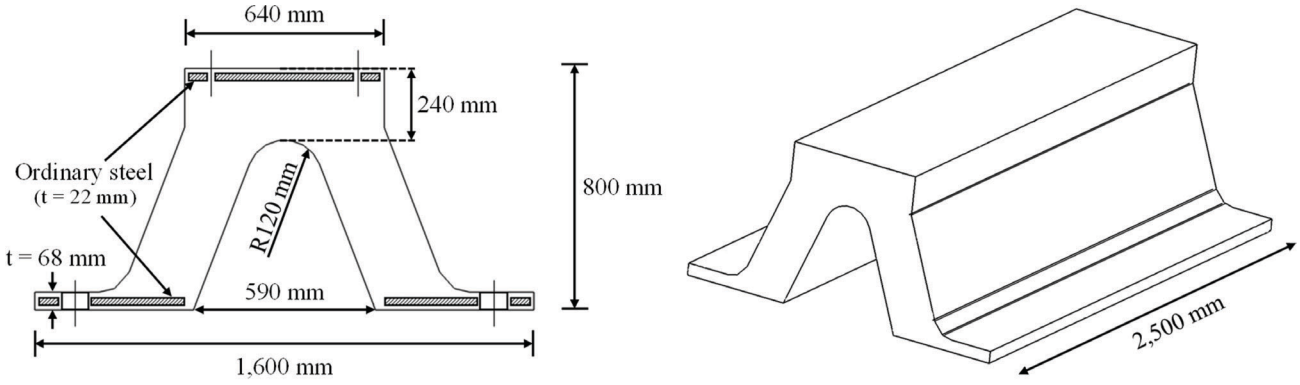

(a) (b)

Figure 15. Dimensions of V-shaped rubber fender used for crushing test: (a) front view, and (b) isometric view

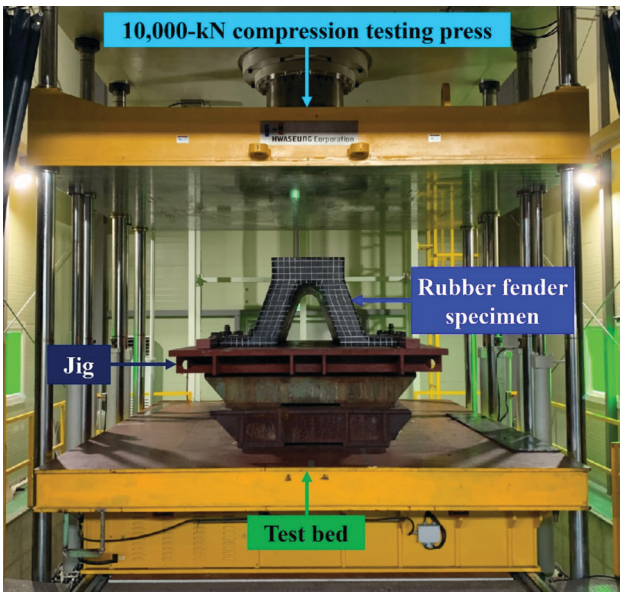

Figure 16. Crushing test set-up of the V-shaped rubber fender before axial compressive loading

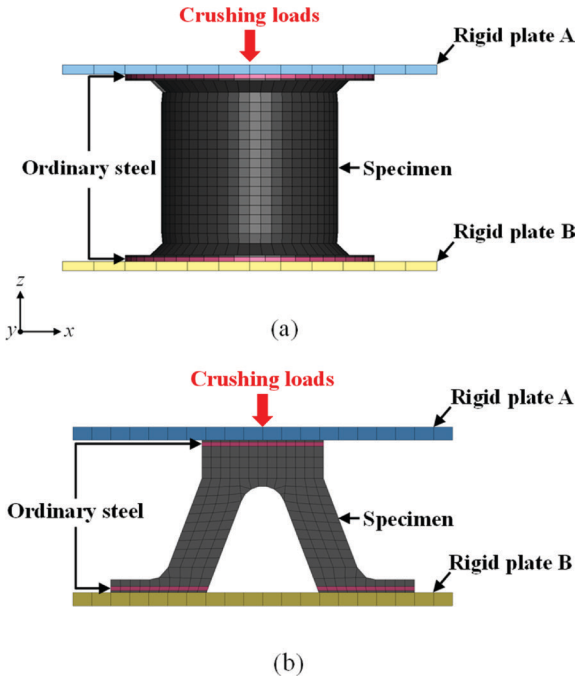

Figure 17. Geometry of elements in finite element simulations using LS-DYNA: (a) circular tube-shaped model, and (b) V-shaped model

3.3 USE OF COMPUTATIONAL MODELLING TECHNIQUES TO MODEL SPECIMEN CRUSHING BEHAVIOUR

The computational modelling techniques presented in Section 2 were used to model the behaviour of specimens in the crushing tests of both the circular tube and V-shaped models. Figure 17 illustrates the geometry of the elements in the finite element simulations performed using the LS-DYNA software package (LS-DYNA, 2021).

Solid cubic elements (regular hexahedra) were employed, and a convergence study of structural responses with varying mesh sizes revealed that the optimum size was 15 mm × 15 mm × 15 mm and 50 mm × 50 mm × 50 mm for the circular tube and V-shaped model test specimens, respectively.

Ordinary steel plate was represented using the 'MAT 24 PIECEWISE_LINEAR_PLASTICITY' model (Kim et al., 2015; Matsui et al., 2018; Paik and Won, 2007; Pineau et al., 2021) and the material properties indicated in Table 1, whereas rubber was modelled using the techniques described in Section 2.

In addition, the 'CONTACT AUTOMATIC SINGLE SURFACE' model was used to prevent self-penetration owing to progressive folding (Fernandez et al., 2022; Ehlers et al., 2012; Sun et al., 2017), and the 'CONTACT AUTOMATIC SURFACE TO SURFACE' model was used to represent the contact condition between the rigid test wall, the ordinary steel plates, and the rubber fender structure.

The crushing load velocity was set to 2,000 mm/s to reduce the computational costs. However, a quasi-static loading scenario was verified according to the principles of Santosa et al. (2000): the total kinetic energy was very small compared with the total internal energy during the crushing simulation, and the force–penetration response was independent of the applied velocity.

3.4 RESULTS AND DISCUSSION

Figure 18 shows deformed shapes of the circular tube-shaped rubber fender model obtained from testing and FEA at four penetration levels: 0 mm (the initial state), 100 mm (after reaching the peak force with crushing), 150 mm (at the end of folding), and 200 mm (the fully crushed state).

Figure 19 shows the force–penetration and the absorbed energy–penetration relationships obtained from the circular tube-shaped model testing and FEA. As shown in Figure 19(a), crushing behaviour was observed in both the test and FEA results: the forces increased until they reached a peak, decreased until the end of folding, and then drastically increased until the fully crushed state was reached.

The computational modelling using uniaxial test data overestimated the energy absorption capacity of the rubber fender, whereas that using the combined test data slightly underestimated this capacity but showed an acceptable level of accuracy.

Figure 20 shows deformed shapes of the V-shaped rubber fender model obtained from testing and FEA at three penetration levels: 0 mm, 100 mm, and 200 mm. Similar to the results of circular tube-shaped model testing, the computational modelling using data from uniaxial tests significantly overestimated the energy absorption capacity of the V-shaped rubber fender, whereas that using a combination of the data from various tests underestimated this capacity but showed an acceptable level of accuracy (Figure 21).

Taken together, the results presented in this section reveal that a combination of data from multiple physical tests of rubber materials should be used in the FEA of rubber fenders, as this affords accurate predictions of their mechanical behaviour and energy absorption capacities.

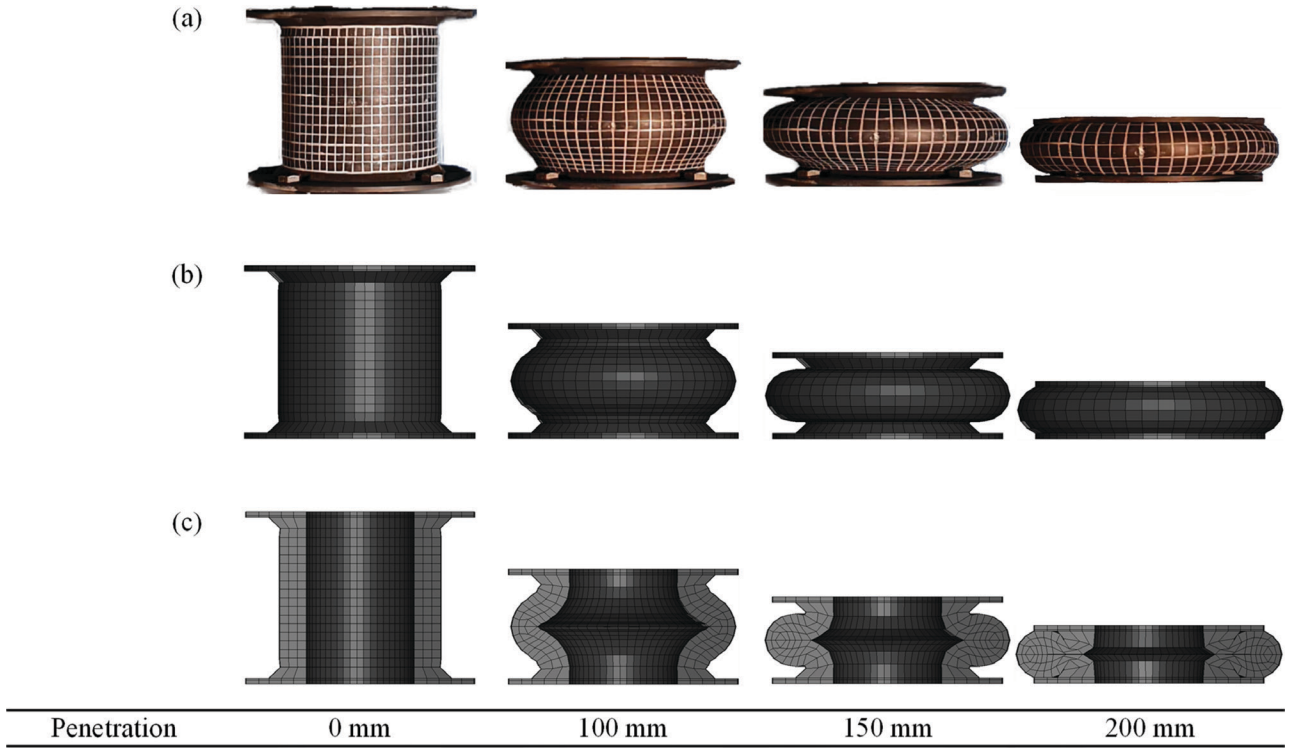

Figure 18. Deformed shapes of the circular tube-shaped rubber fender model obtained from testing and finite element analysis (FEA) at different penetration levels: (a) test, (b) FEA, and (c) cross-sectional view of (b)

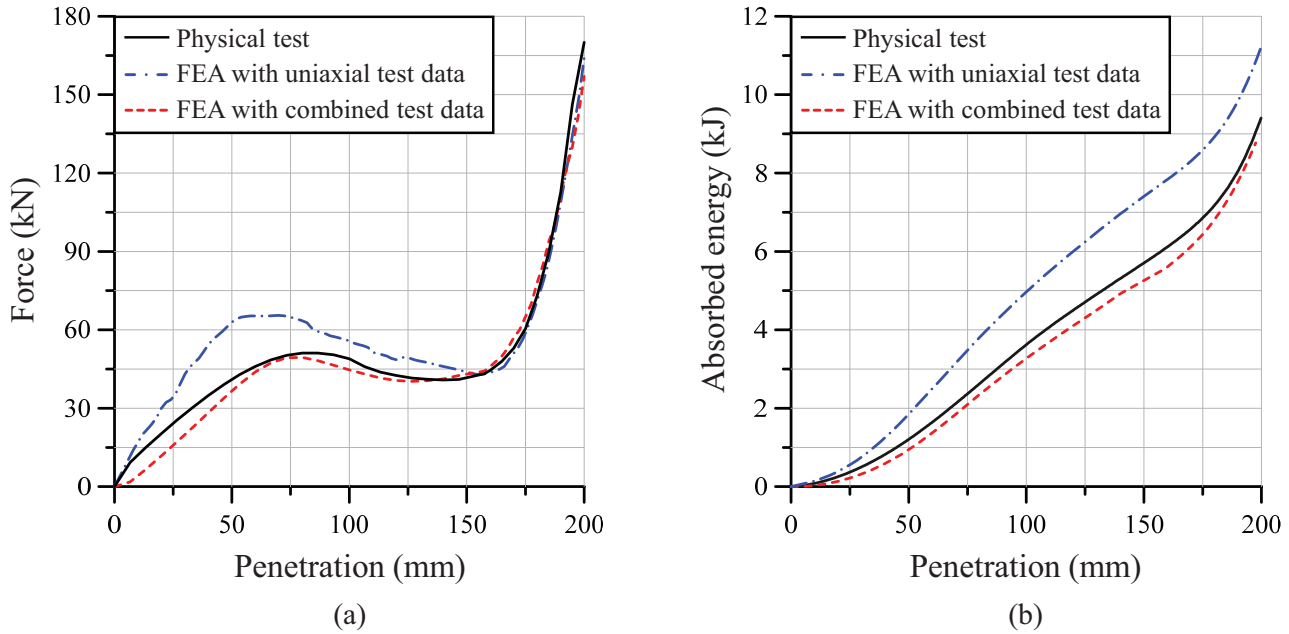

Figure 19. Comparison of the circular tube-shaped rubber fender model testing versus finite element analysis: (a) force–penetration relationship, and (b) absorbed energy–penetration relationship (FEA = finite element analysis)

For both the circular tube-shaped rubber fender model with a simple geometry and the V-shaped rubber fender model with a complex geometry, the computational models developed in the present study give accurate results compared to the test data as far as the constitutive model of materials considering the combined load effect is applied.

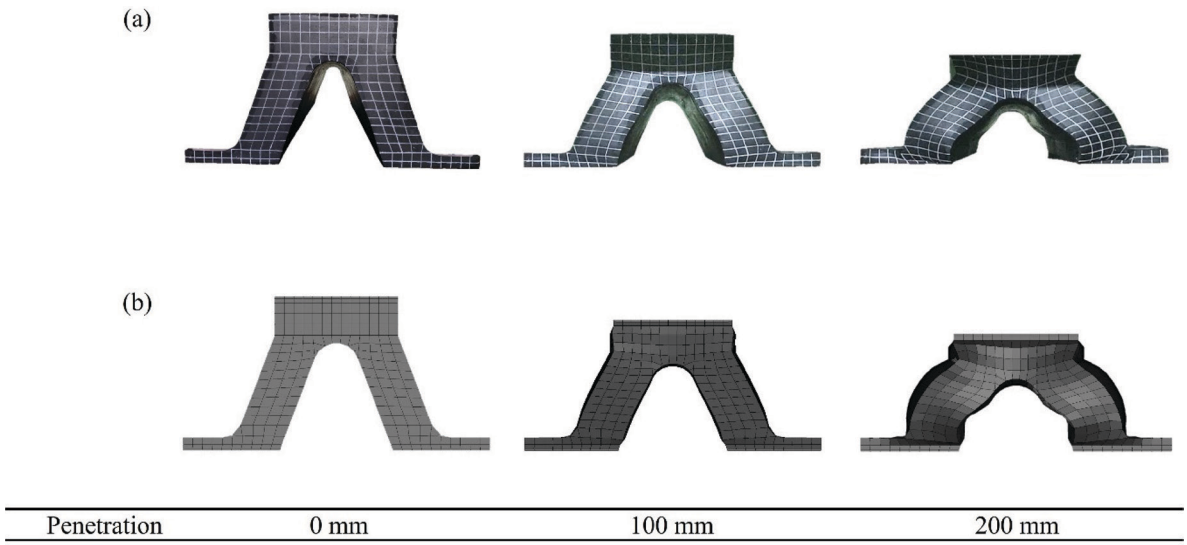

Figure 20. Deformed shapes of the V-shaped rubber fender model obtained from testing and finite element analysis (FEA) at various penetration levels: (a) test, and (b) FEA

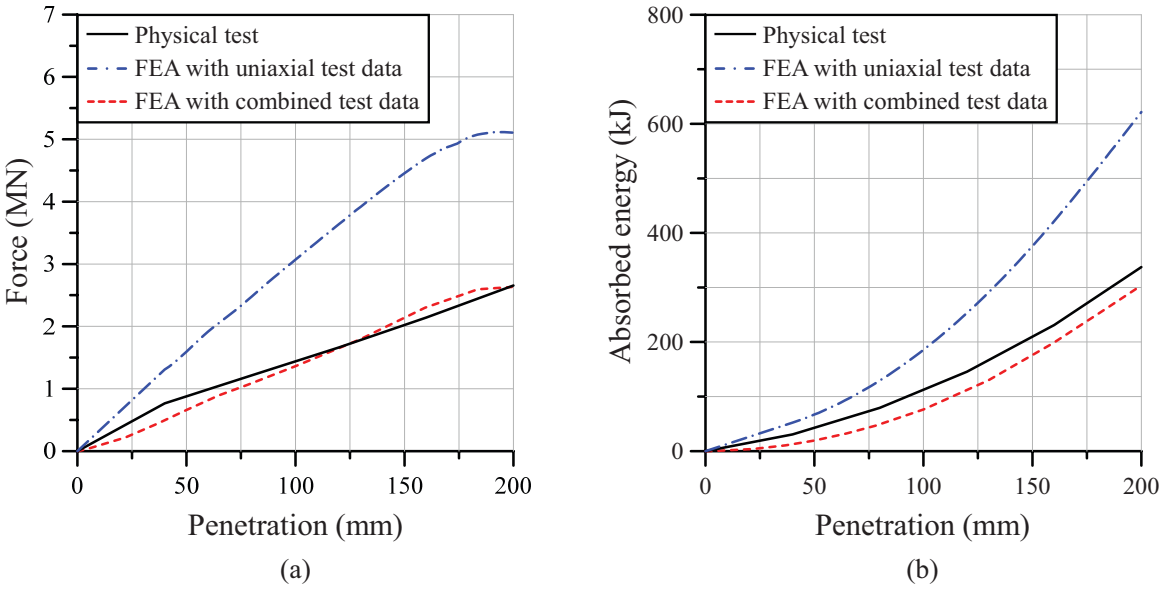

Figure 21. Comparison of the V-shaped rubber fender model testing versus finite element analysis: (a) force–penetration relationship, and (b) absorbed energy–penetration relationship (FEA = finite element analysis)

4. CASE STUDIES: LOW-SPEED COLLISION BETWEEN AN FPSO UNIT HULL AND A SHUTTLE TANKER WORKING SIDE-BY-SIDE IN OFFLOADING OPERATIONS

The ability of V-shaped rubber fenders to prevent structural damage resulting from low-speed collisions was evaluated by applying the developed computational models to a simulation of a collision between a VLCC class FPSO unit hull and a Suezmax class shuttle tanker, in which the latter was considered the striking object (Figure 22). Table 3 presents the principal dimensions of the FPSO unit hull and the shuttle tanker.

Table 3. Principal dimensions of the FPSO unit and the shuttle tanker

Parameter	FPSO	Shuttle tanker
Overall length (m)	305.0	270.2
Breadth (m)	60.0	48.0
Depth (m)	30.0	23.7
Draught (m)	21.6	16.0
Deadweight (tonne)	334,500	157,500
Transverse frame spacing (m)	5.69	4.80

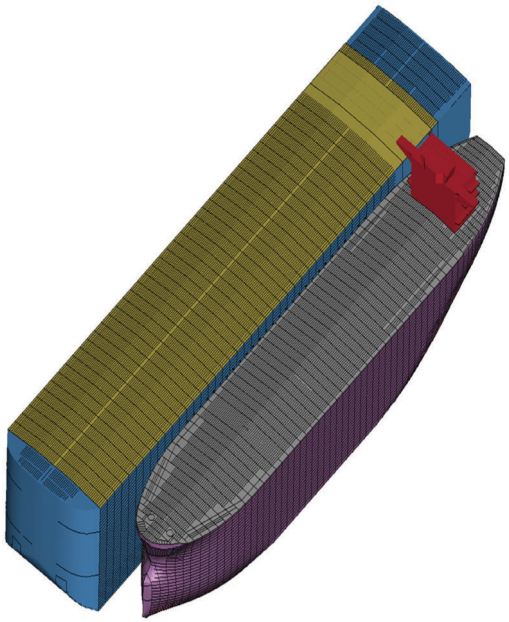

Figure 22. Model of a side-by-side collision between a VLCC class FPSO unit hull and a Suezmax class shuttle tanker

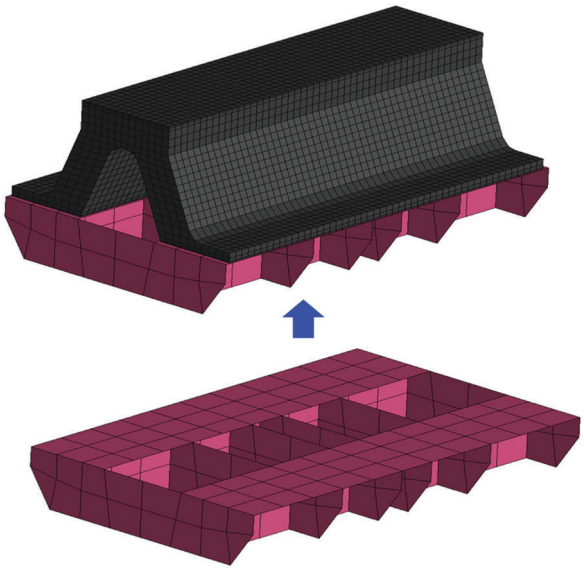

Figure 23. Finite element models of a V-shaped rubber fender and a fender seat

4.1 STRUCTURAL MODELLING OF RUBBER FENDERS

V-type rubber fenders that had the same geometry and material properties as the V-shaped rubber fender test model described in Section 3.2 were modelled together with the supporting structures (fender seats). This is in accordance with industrial practice (Figure 23), in which fender seats are welded at side hull plates supported by transverse frames. The total length of side shell plates equipped with rubber fenders was 141.6 m, which spans the expected collision zone shown in Figure 24.

4.2 STRUCTURAL MODELLING OF STRIKING AND STRUCK HULL STRUCTURES

Structural modelling of the striking (shuttle tanker) and struck (FPSO unit) hull structures was conducted using LS-DYNA, in accordance with the work of Park et al. (2023), with the two hull structures regarded as consisting of mild or AH32 high-tensile steel. The measured material properties in the MPDAS database (Paik et al., 2017a) were used to model the structures (Table 4). Finite element modelling of the plating and support members was performed with only plate-shell elements.

Instead of a convergence study, a practical study was performed using a simplified method that has been devised by Paik to determine the appropriate size for a plate-shell element (Paik, 2007a, 2007b, 2018, 2020, 2022). This revealed that the required element size was 220 mm (fine meshes) for the collision area, and 880 mm (coarse meshes) elsewhere. Table 5 summarises the determined element types, sizes, and the number of elements in the FPSO unit hull, the shuttle tanker, the V-type rubber fenders, and the fender seats.

The effects of strain rate on the mechanical properties of the steels were not considered because the numerical simulations were performed in a quasi-static scenario. Critical fracture strain was used for nonlinear FEA under quasi-static loading conditions (Hughes and Paik, 2010; Ko et al., 2018b; Paik, 2020, 2022).

Table 4. Material properties used for the analysis (Park et al., 2023)

Material property (unit)	Mild steel	AH32 high-tensile steel
Density, ρ (ton/m^3)	7.85	7.85
Young's modulus, E (MPa)	205,800	205,800
Poisson's ratio, ν	0.3	0.3
Yield stress, σ_Y (MPa)	281.57	400.97
Static fracture strain, ε_f	0.429	0.324
Critical fracture strain, ε_{fc}	0.120	0.099

The critical fracture strains were determined by Equation (3), as follows, and were 0.120 for mild steel and 0.099 for AH32 high-tensile steel, respectively (Paik, 2018):

$$\varepsilon_{fc} = \gamma d_1 \left(\frac{t}{s}\right)^{d_2} \varepsilon_f \tag{3}$$

Table 5. Element types and the number of elements used in finite element structural modelling

Structure	Element type	No. of fine elements (element size)	No. of coarse elements (element size)	Total
FPSO unit hull	Plate-shell	858,603 (220 mm × 220 mm)	300,786 (880 mm × 880 mm)	1,159,389
Shuttle tanker	Plate-shell	342,686 (220 mm × 220 mm)	184,221 (880 mm × 880 mm)	526,907
Rubber fender	Solid (cube type)	582,400 (50 mm × 50 mm × 50 mm)	–	582,400
Fender seat	Plate-shell	12,064 (220 mm × 220 mm)	–	12,064

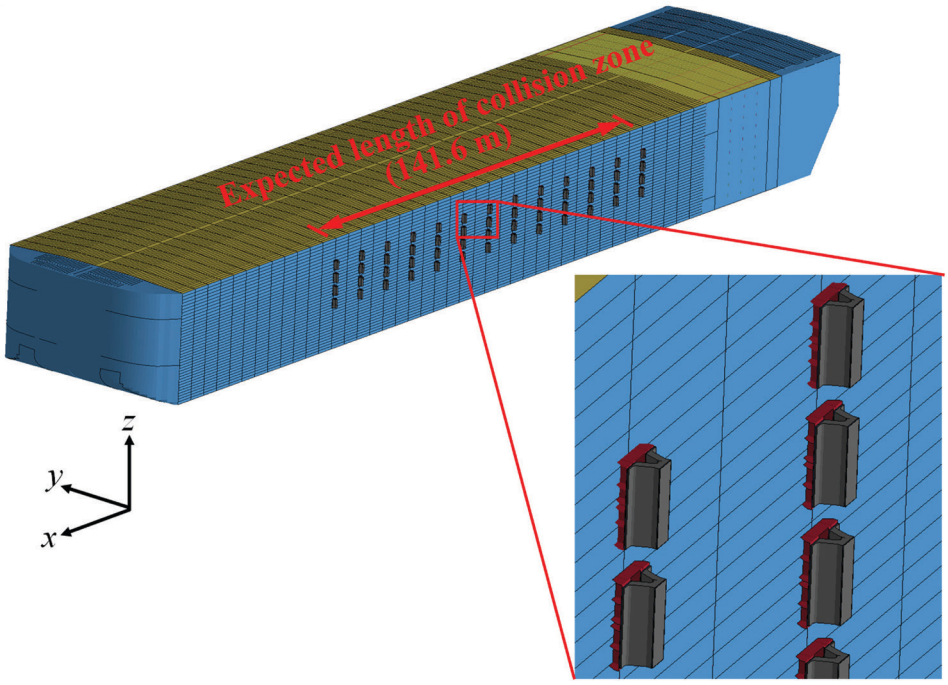

Figure 24. Geometry of an FPSO unit hull equipped with V-shaped rubber fenders

where ε_f is the static fracture strain, t is the plate thickness, and s is the mesh size. The plate thicknesses of the striking and struck hull structures were 17 and 20 mm, respectively; the mesh size was $s = 220\,\text{mm}$; and the constants in Equation 3 were $\gamma = 0.3$, $d_1 = 4.1$, and $d_2 = 0.58$.

4.3 RESULTS AND DISCUSSION

No major collision damage (i.e., no visible damage) was observed on the striking and struck hull structures in either collision scenario, i.e., in the absence or presence of rubber fenders on the FPSO unit hull. Figures 25 and 26 show the changes in the energy absorbed by the FPSO unit and shuttle tanker hulls in the absence and in the presence of rubber fenders, respectively, at a side-by-side collision speed of 0.5 kt. The computational models presented in section 2 were applied in this case study and are compared in Figure 26.

In the absence of rubber fenders, the FPSO unit and the shuttle tanker hulls temporarily absorbed a maximum of 43.9% and 22.8% of the initial kinetic energy during the collision, respectively. However, the kinetic energy rebounded at approximately 0.1 s, at which time the energies absorbed by the FPSO unit and the shuttle tanker hulls simultaneously and significantly decreased. The energy remaining after 0.2 s represented the plastic deformation that occurred in the FPSO unit and the shuttle tanker hull structures, although this structural damage was not visually observed. The energy remaining in the FPSO unit hull and the shuttle tanker accounted for 10.2% and 5.3% of the initial kinetic energy, respectively.

In the presence of rubber fenders, little energy was absorbed by the hulls during the collision; most was absorbed by the fenders. Moreover, there was no plastic deformation in the FPSO unit hull or the shuttle tanker hull (i.e., no energy remained in these hulls after the collision), as shown in Figures 26 and 27, such that the rebounded

kinetic energies after the collision were higher than those in the absence of rubber fenders.

The amount of energy absorbed by the rubber fenders fluctuated after the collision because they underwent repeated deformation and recovery for a certain period after the collision. There were significant differences between the computational model based on a combination of data from various tests and that based on data from uniaxial tests; due to lower stiffness (or higher deformability), the former model determined that the fenders had greater energy-absorption capacity than did the latter model.

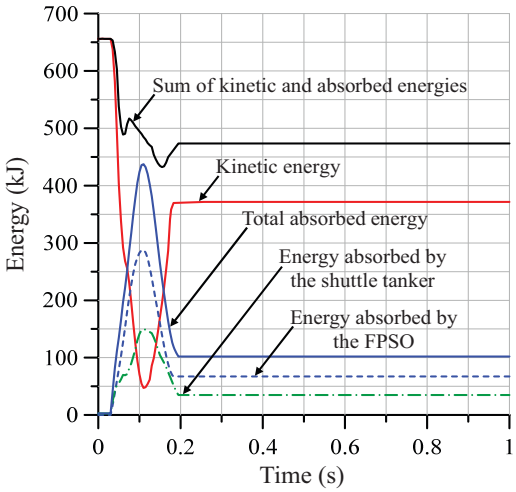

Figure 25. Change in absorbed energies over time in the FPSO unit hull without rubber fenders and the shuttle tanker hull in a 0.5 kt side-by-side collision scenario

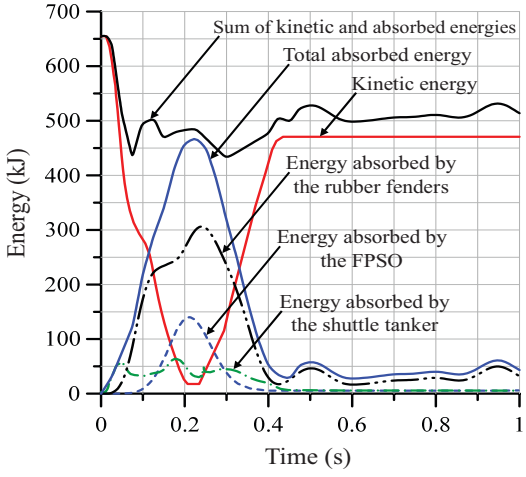

Figure 26. Change in absorbed energies over time in the FPSO unit hull with rubber fenders and the shuttle tanker hull in a 0.5 kt side-by-side collision scenario, when the constitutive model of rubber material is used with the uniaxial tensile load effect alone

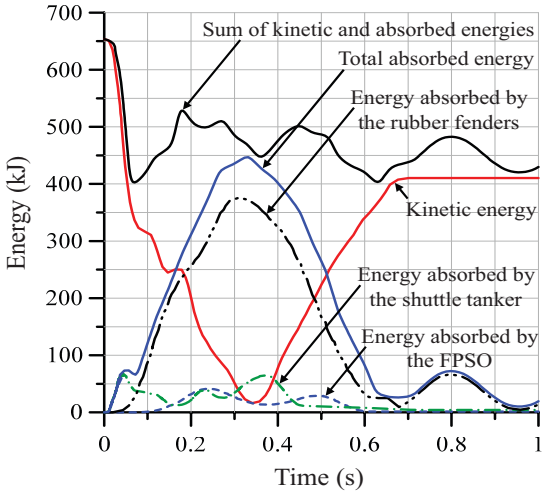

Figure 27. Change in absorbed energies over time in the FPSO unit hull with rubber fenders and the shuttle tanker hull in a 0.5 kt side-by-side collision scenario, when the constitutive model of rubber material is used with the combined load effect

5. CONCLUDING REMARKS

This study evaluated the ability of solid rubber fenders to prevent structural damage due to low-speed collisions between an FPSO unit hull and a shuttle tanker working side-by-side in offloading operations.

Computational modelling techniques were developed and validated by comparison with data from tests of physical models, which enabled the finite element method to be used for the accurate evaluation of the protective effect of rubber fenders. Computational models were used in case studies in which a shuttle tanker collided with an FPSO unit hull, with was equipped and not equipped with rubber fenders, respectively. The conclusions are summarised as follows.

1. Two computational models of rubber were developed and validated by a comparison with physical model test data, and then used to evaluate the energy absorption capacity of rubber fenders.
2. The physical model tests were performed on a circular tube-shaped model and a V-shaped model in accordance with industrial practice.
3. Compared with test data, the computational model based on a combination of data from various tests showed an acceptable level of accuracy in its estimates of the energy absorption capacity of rubber fenders, but that based on data from uniaxial tests generated overestimates.
4. The developed computational models were applied to examine a case study of a low-speed (0.5 kt) collision between a Suezmax class shuttle tanker and a VLCC class FPSO unit hull equipped or not equipped with rubber fenders, respectively. When the FPSO unit

hull was not equipped with rubber fenders, the FPSO hull and that of the shuttle tanker exhibited plastic deformation (as energy remained) after the collision, whereas when the FPSO unit hull was equipped with rubber fenders, neither of the hulls exhibited plastic deformation (as no energy remained) after the collision.

5. The effect of combined loads on the constitutive model of rubber materials is significant, as evident from the validation of the computational models by comparison with physical test results. The computational modelling of rubber materials should then be developed by taking into account the combined load effect rather than using the data obtained from uniaxial tensile tests alone.
6. The results show that the developed computational modelling techniques are useful for analysing the energy absorption capacity of solid rubber fenders under relatively low-speed collision loading conditions.
7. The effect of strain rates on the mechanical properties of materials such as steels or rubbers is obvious in high-speed collision cases. Further studies are required and a sequel to this paper is ongoing.

6. ACKNOWLEDGEMENTS

This work was supported by BK21 FOUR Program by Pusan National University Research Grant, 2021. The authors thank Hwaseung Corporation for providing rubber fender specimens for use in physical testing. The authors also thank Hye Rim Cho, Dae Kyeom Park, and Soung Woo Park at the Korea Ship and Offshore Research Institute (Lloyd's Register Foundation Research Centre of Excellence), Pusan National University, for their assistance with the small-scale physical model testing.

7. ORCIDS

Hyeong Jin Kim
https://orcid.org/0000-0001-5344-3209

Sang Min Park
https://orcid.org/0000-0003-0040-3486

Giles Thomas
https://orcid.org/0000-0002-6122-4329

Jeom Kee Paik
https://orcid.org/0000-0003-2956-9359

8. REFERENCES

1. AKIYAMA, H., SHIMIZU, K., UEDA, S., and KAMADA, T. (2017a) *Investigation on service years of large rubber marine fenders*. Journal of Japan Society of Civil Engineers. 5: 392–401.
2. AKIYAMA, H., SHIOMI, T., OMURA, A., YAMAMOTO, S., UEDA, S., and KAMADA, T. (2017b) *Method to estimate the aging of large rubber marine fender*. 27th International Ocean and Polar Engineering Conference, San Francisco, California, USA, June 25–30.
3. ALI, A., HOSSEINI, M., and SAHARI, B.B. (2010) *A review and comparison on some rubber elasticity models*. Journal of Scientific & Industrial Research. 69: 495–500.
4. ALI, A.M., ESSA, M.J.K., and HASSAN, A.Q. (2017) *Evaluate the cylindrical rubber fender response under dynamic load*. 7th International Conference on Advances in Civil and Structural Engineering – CSE 2017, Kuala Lumpur, Malaysia, July 1–2.
5. BABALEYE, A.O. and KURT, R.E. (2020) *Safety analysis of offshore decommissioning operation through Bayesian network*. Ships and Offshore Structures. 15 (1): 99–109.
6. BEDA, T. (2007) *Modeling hyperelastic behavior of rubber: A novel invariant-based and a review of constitutive models*. Journal of Polymer Science: Part B, Polymer Physics. 45: 1713–1732.
7. BEDA, T. (2014) *An approach for hyperelastic model-building and parameters estimation a review of constitutive models*. European Polymer Journal. 50: 97–108.
8. BÖL, M. and REESE, S. (2006) *Finite element modelling of rubber-like polymers based on chain statistics*. International Journal of Solids and Structures. 43 (1): 2–26.
9. CEFOR (2021) *Annual report 2021*. The Nordic Association of Marine Insurers, Oslo, Norway.
10. CHEN, T.L., WU, H., and FANG, Q. (2022) *Impact force models for bridge under barge collisions*. Ocean Engineering. 259: 111856.
11. CHO, H.R., KIM, H.J., PARK, S.M., PARK, D.K., YUN, S.H., and PAIK, J.K. (2023) *Effect of solid rubber fenders on the structural damage due to collisions between a ship-shaped offshore installation and an offshore supply vessel*. Ships and Offshore Structures. 18(7): 1037–1059.
12. DAL, H., AÇIKGÖZ, K., and BADIENIA, Y. (2021) *On the performance of isotropic hyperelastic constitutive models for rubber-like materials: a state of the art review*. Applied Mechanics Reviews. 73 (2): 020802.
13. DEEB, H., MEHDI, R.A., and HAHN, A. (2017) *A review of damage assessment models in the maritime domain*. Ships and Offshore Structures. 12 (S1): 31–54.
14. DEKKER, R. and WALTERS, C.L. (2017) *A global FE–local analytical approach to modelling failure in localised buckles caused by crash*. Ships and Offshore Structures. 12 (S1): 1–10.
15. EHLERS, S., TABRI, K., ROMANOFF, J., and VARSTA, P. (2012) *Numerical and experimental*

investigation on the collision resistance of the X-core structure. Ships and Offshore Structures. 7 (1): 21–29.

16. ENGELBREKTSSON, K. (2011) *Evaluation of material models in LS-DYNA for impact simulation of white adipose tissue*. Master's Thesis, Chalmers University of Technology, Sweden.
17. FAISAL, M., NOH, S.H., KAWSAR, M.R.U., YOUSSEF, S.A.M., SEO, J.K., HA, Y.C., and PAIK, J.K. (2017) *Rapid hull collapse strength calculations of double hull oil tankers after collisions*. Ships and Offshore Structures. 12 (5): 624–639.
18. FERNANDEZ, J.M., VAZ, M.A., and CYRINO, J.C.R. (2022) *Numerical study on the collision of platform supply vessel and floating production storage and offloading platform*. Ships and Offshore Structures. 17 (7): 1485–1497.
19. HARIS, S. and AMDAHL, J. (2012) *An analytical model to assess a ship side during a collision*. Ships and Offshore Structures. 7 (4): 431–448.
20. HE, H., ZHANG, Q., ZHANG, Y., CHEN, J., ZHANG, L., and LI, F. (2022) *A comparative study of 85 hyperelastic constitutive models for both unfilled rubber and highly filled rubber nanocomposite material*. Nano Materials Science. 4 (2): 64–82.
21. HUGHES, O.F. and PAIK, J.K. (2010) *Ship structural analysis and design*. The Society of Naval Architectures and Marine Engineers, Alexandria, Virginia, USA. ISBN: 978-0-939773-78-3.
22. INSTRON (2005) *Instron series 5500 load frames including series 5540, 5560, 5580: reference manual – equipment. M10-14190-EN*. Instron Corporation, Norwood, Massachusetts, USA.
23. INSTRON (2020) *Specification: AVE 2 – non-contacting video extensometer*. Instron Corporation, Norwood, Massachusetts, USA.
24. ISO (2017) *ISO 37: Rubber, vulcanized or thermoplastic – determination of tensile stress-strain properties*. International Organization for Standardization, Vernier, Geneva, Switzerland.
25. JONES, N. and PAIK, J.K. (2013) *Impact perforation of steel plates*. Ships and Offshore Structures. 8 (5): 579–596.
26. KIM, S.J., SEO, J.K., MA, K.Y., and PARK, J.S. (2021) *Methodology for collision-frequency analysis of wind-turbine installation vessels*. Ships and Offshore Structures. 16 (4): 423–439.
27. KIM, W.-D., KIM, W.-S., KIM, D.-J., WOO, C.-S., and LEE, H.-J. (2004) *Mechanical testing and nonlinear material properties for finite element analysis of rubber components*. Transactions of the Korean Society of Mechanical Engineers A. 28 (6): 848–859.
28. KIM, Y.S., YOUSSEF, S., INCE, S., KIM, S.J., SEO, J.K., KIM, B.J., HA, Y.C., and PAIK, J.K. (2015) *Environmental consequences associated with collisions involving double hull oil tanker*. Ships and Offshore Structures. 10 (5): 479–487.
29. KO, Y.G., KIM, S.J., and PAIK, J.K. (2018a) *Effects of a deformable striking ship's bow on the structural crashworthiness in ship-ship collisions*. Ships and Offshore Structures. 13 (S1): 228–250.
30. KO, Y.G., KIM, S.J., SOHN, J.M., and PAIK, J.K. (2018b) *A practical method to determine the dynamic fracture strain for the nonlinear finite*. Ships and Offshore Structures. 13 (4): 412–422.
31. LADEIRA, I., MÁRQUEZ, L., ECHEVERRY, S., SOURNE, H.L., and RIGO, P. (2022) *Review of methods to assess the structural response of offshore wind turbines subjected to ship impacts*. Ships and Offshore Structures. 18(6): 755–774.
32. LARABA-ABBES, F., IENNY, P., and PIQUES, R. (2003) *A new 'tailor-made' methodology for the mechanical behaviour analysis of rubber-like materials: II. Application to the hyperelastic behaviour characterization of a carbon-black filled natural rubber vulcanizate*. Polymer. 44 (3): 821–840.
33. LEE, K. (2013) *Effects on the various rubber fenders of a tripod offshore wind turbine substructure collision strength due to boat*. Ocean Engineering. 72: 188–194.
34. LEE, K.-S. and PARK, R.-S. (2012) *Effective arrangement of rubber fenders of wind-measuring met mast due to boat*. International Journal of Offshore and Polar Engineering. 22 (1): 69–75.
35. LINDLEY, T.B. (1974) *Engineering design with natural rubber*. Fourth Edition. The Malaysian Rubber Producers Research Association, Hertford, UK.
36. LIU, K., LIU, B., VILLAVICENCIO, R., WANG, Z., and GUEDES SOARES, C. (2018) *Assessment of material strain rate effects on square steel plates under lateral dynamic impact loads*. Ships and Offshore Structures. 13 (2): 217–225.
37. LS-DYNA (2021) *Keyword user's manual – volume I*. Livermore Software Technology, Livermore, California, USA.
38. MATSUI, S., UTO, S., YAMADA, Y., and WATANABE, S. (2018) *Numerical study on the structural response of energy-saving device of ice-class vessel due to impact of ice block*. International Journal of Naval Architecture and Ocean Engineering. 10 (3): 367–375.
39. MELLY, S.K., LIU, L., LIU, Y., and LENG, J. (2021) *A review on material models for isotropic hyperelasticity*. International Journal of Mechanical System Dynamics. 1 (1): 71–88.
40. MULLINS, L. (1969) *Softening of rubber by deformation*. Rubber Chemistry and Technology. 42 (1): 339–362.

41. OILNOW (2023) Petrobras to add 14 FPSOs offshore Brazil in next four years. Available at: https://oilnow.gy/featured/petrobras-to-add-14-fpsos-offshore-brazil-in-next-four-years/ (Accessed 14th July 2023).
42. PAIK, J.K. (2007a) *Practical techniques for finite element modeling to simulate structural crashworthiness in ship collisions and grounding (Part I: Theory)*. Ships and Offshore Structures. 2 (1): 69–80.
43. PAIK, J.K. (2007b) *Practical techniques for finite element modelling to simulate structural crashworthiness in ship collisions and grounding (Part II: Verification)*. Ships and Offshore Structures. 2 (1): 81–85.
44. PAIK, J.K. (2018) *Ultimate limit state analysis and design of plated structures*. 2nd Ed. John Wiley & Sons, Chichester, UK. ISBN: 978-111-93-6779-6.
45. PAIK, J.K. (2020) Advanced structural safety studies with extreme conditions and accidents. Springer, Singapore. ISBN: 978-981-13-8244-4.
46. PAIK, J.K. (2022) Ship-shaped offshore installations: design, construction, operation, healthcare, and decommissioning. 2nd Ed. Cambridge University Press, Cambridge, UK. ISBN: 978-131-65-1960-8.
47. PAIK, J.K., KIM, K.J., LEE, J.H., JUNG, B.G., and KIM, S.J. (2017a) *Test database of the mechanical properties of mild, high-tensile and stainless steel and aluminium alloy associated with cold temperatures and strain rates*. Ships and Offshore Structures. 12 (S1): 230–256.
48. PAIK, J.K., KIM, S.J., KO, Y.G., and YOUSSEF, S.A.M. (2017b) Collision risk assessment of a VLCC class tanker. SNAME Maritime Convention, Houston, Texas, USA, October 24–28.
49. PAIK, J.K. and THAYAMBALLI, A.K. (2006) *Some recent developments on ultimate limit state design technology for ships and offshore structures*. Ships and Offshore Structures. 1 (2): 99–116.
50. PAIK, J.K. and WON, S.H. (2007) *On deformation and perforation of ship structures under ballistic impacts*. Ships and Offshore Structures. 2 (3): 217–226.
51. PAN, J., WANG T., ZHANG, W.Z., HUANG S.W., and XU, M.C. (2022) *Study on the assessment of axial crushing force of bulbous bow for bridge against ship collision*. Ocean Engineering. 255: 111411.
52. PARK, S.M., KIM, H.J., CHO, H.R., KONG, K.H., PARK, D.K., and PAIK, J.K. (2023) *Effect of pneumatic rubber fenders on the prevention of structural damage during collisions between a ship-shaped offshore installation and a shuttle tanker working side-by-side*. Ships and Offshore Structures. 18(4): 596–608.
53. PIANC (2002) *Guidelines for the design of fender systems. Report of Working Group 33 of the Maritime Navigation Commission*. International Navigation Association, Brussels, Belgium.
54. PINEAU, J.P., LE SOURNE, H., and SOULHI Z. (2021) *Rapid assessment of ship raking grounding on elliptic paraboloid shaped rock*. Ships and Offshore Structures. 16 (S1): 106–121.
55. QUINTON, B.W.T., DALEY, C.G., GAGNON, R.E., and COLBOURNE, D.B. (2017) *Guidelines for the nonlinear finite element analysis of hull response to moving loads on ships and offshore structures*. Ships and Offshore Structures. 12 (S1): 109–114.
56. RUDAN, S., KARAČIĆ, J., and ĆATIPOVIĆ, I. (2021) *Non-linear response of a moored LNG ship subjected to regular waves*. Ships and Offshore Structures. 16 (S1): 44–57.
57. SAIDOU, A., GAURON, O., BUSSON, A., and PAULTRE, P. (2021) *High-order finite element model of bridge rubber bearings for the prediction of buckling and shear failure*. Engineering Structures. 240: 112314.
58. SAMUELIDES, M. (2015) *Recent advances and future trends in structural crashworthiness of ship structures subjected to impact loads*. Ships and Offshore Structures. 10 (5): 488–497.
59. SANTOSA, S.P., WIERZBICKI, T., HANSSEN, A.G., and LANGSETH, M. (2000) *Experimental and numerical studies of foam-filled sections*. International Journal of Impact Engineering. 24 (5): 509–534.
60. SHA, Y. and AMDAHL, J. (2019) *A simplified analytical method for predictions of ship deckhouse collision loads on steel bridge girders*. Ships and Offshore Structures. 14 (S1): 121–134.
61. SHEN, M.-Y., CHIOU, Y.-C., TAN, C.-M., WU, C.-C., and CHEN, W.-J. (2020) *Effect of wall thickness on stress-strain response and buckling behavior of hollow-cylinder rubber fenders*. Materials. 13 (5): 1170.
62. SHEN, M.-Y., WU, C.-C., and CHIOU Y.-C. (2022) *Enhance energy absorption of hollow-cylinder rubber fender using V-notch ring grooves*. Ocean Engineering. 255: 111442.
63. SHOKRGOZAR, H.R., ASGARIAN, B., and AGHAEIDOOST, V. (2022) *Experimental investigation of decomposition of signal energy for damage detection of jacket type offshore platforms*. Ships and Offshore Structures. 17 (9): 2012–2022.
64. SONG, Y. and WANG, J. (2019) *Development of the impact force time-history for determining the responses of bridges subjected to ship collisions*. Ocean Engineering. 187: 106182.
65. STORHEIM, M. and AMDAHL, J. (2017) *On the sensitivity to work hardening and strain-rate effects in nonlinear FEM analysis of ship*

collisions. Ships and Offshore Structures. 12 (1): 100–115.

66. SUN, L., ZHANG, Q., MA, G., and ZHANG, T. (2017) *Analysis of ship collision damage by combining Monte Carlo simulation and the artificial neural network approach*. Ships and Offshore Structures. 12 (S1): 21–30.
67. TRELLEBORG (2023) Hull fenders. Available at: www.trelleborg.com/en/marine-and-infrastructure/products-solutions-and-services/marine/marine-fenders/fixed-fenders/hull-fender/ (Accessed 14th July 2023).
68. WOO, C.-S. (2019) *Strain energy function for finite element analysis of rubber components*. Rubber Technology. 20 (2): 94–101.
69. WOO, C.S. and PARK, H. (2019) *Rubber material properties test and evaluation for automobile suspension bush*. Transactions of the Korean Society of Automotive Engineers. 27 (8): 595–602.
70. WOO, C.S., KIM, W.D., KIM, K.S., and KWON, J.D. (2002) *An experimental study on the dynamic characteristics of rubber isolator*. Elastomer. 37 (3): 183–191.
71. WU, B., YIP, T.L., YAN, X., GUEDES SOARES, C. (2019) *Fuzzy logic based approach for ship-bridge collision alert system*. Ocean Engineering. 187: 106152.
72. WU, C.-C. and CHIOU, Y.-C. (2019) *Stress-strain response of cylindrical rubber fender under monotonic and cyclic compression*. Materials. 12 (2): 282.
73. YAN, L., DILLARD, D.A., WEST, R.L., LOWER, L.D., and GORDON, G.V. (2010) *Mullins effect recovery of a nanoparticle-filled polymer*. Journal of Polymer Science: Part B, Polymer Physics. 48: 2207–2214.
74. YOUSSEF, S.A.M., FAISAL, M., SEO, J.K., KIM, B.J., HA, Y.C., KIM, D.K., PAIK, J.K., CHENG, F., and KIM, M.S. (2016) *Assessing the risk of ship hull collapse due to collision*. Ships and Offshore Structures. 11 (4): 335–350.
75. YU, Z., LIU, Z., and AMDAHL, J. (2019) *Discussion of assumptions behind the external dynamic models in ship collisions and groundings*. Ships and Offshore Structures. 14 (S1): 45–62.
76. ZHANG, M.-G., XU, W., WU, T., ZHANG, X.-D., ZHANG, H., LI, Z., ZHANG, C., JIANG, H., and CHEN, M. (2021) *Investigation on Mullins effect of rubber materials by spherical indentation method*. Forces in Mechanics. 4: 100037.
77. ZHANG, S., PEDERSEN, P.T., and OCAKLI, H. (2015) *Collisions damage assessment of ships and jack-up rigs*. Ships and Offshore Structures. 10 (5): 470–478.
78. ZHANG, W., JIN, X., and WANG, J. (2014) *Numerical analysis of ship–bridge collision's influences on the running safety of moving rail train*. Ships and Offshore Structures. 9 (5): 498–513.

